Journal of Materials Chemistry A

Accepted Manuscript

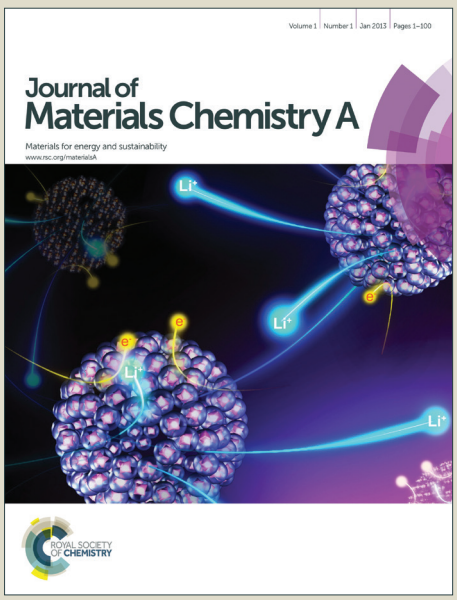

ROYAL SOCIETY OF CHEMISTRY

www.rsc.org/materialsA

High-efficiency Solid-state Polymer Electrolyte Dye-sensitized Solar Cells with a Bi-functional Porous Layer

Woohyung Cho[a], Young Rae Kim[a], Donghoon Song[a], Hyung Woo Choi[a] and Yong Soo Kang[a,*]

[a] Center for Next Generation Dye-sensitized Solar Cells, WCU Department of Energy Engineering, Hanyang University, 133-791, Seoul, Republic of Korea; E-mail: kangys@hanyang.ac.kr; Fax: +82 2 2296 2969; Tel: +82 2 2220 2336

[Abstract]

A simple and effective avenue to increase the energy conversion efficiency is proposed and demonstrated by increasing the ion flux with a reduction in the thickness of the solid polymer electrolyte layer and the mass transport distance of I^-/I_3^- redox couples. Solid-state dye-sensitized solar cells employing polymer electrolyte and a bifunctional insulating layer show a power conversion efficiency of 8.9 % at 1 sun conditions.

[Introduction]

Dye-sensitized solar cells (DSCs) have received much attention due to their attractive features such as high energy conversion efficiency and low production costs. The highest recorded conversion efficiency of 12.3 %[1] was achieved with YD-*o*-C8 dye and cobalt complex redox couples dissolved in liquid acetonitrile; however, the practicability of this complex remains a challenge. For instance, liquid electrolyte-based DSCs face challenges of operational stability and long-term durability associated with the liquid used.[2] Therefore, there have been several approaches to utilize room-temperature ionic liquids,[3] solid-state polymer electrolytes[5] and hole transfer materials[4, 5] for overcoming liquid electrolyte problems. Among them, solid polymer electrolytes (SPEs) are a promising alternative. However, the conversion efficiency of polymer electrolytes was found to be much lower than that of liquid electrolyte mostly because of the low ionic conductivity of the redox species in the polymer matrix and incomplete pore filling in the mesoporous TiO_2 film.

Therefore, there have been several different approaches to improve the ionic conductivity through SPEs. For example, the ionic conductivity of an SPE can be readily improved by incorporating nano-sized inorganic materials mainly due the generation of free volume at the interface between the SPE and nanoparticles.[6-7] The addition of nanoparticles may also inhibit the crystallization of polymer and consequently enhance its ionic conductivity.[6, 7] Weak pore penetration or filling of solid polymer electrolyte has been improved by utilizing small-sized oligomers and subsequent self-solidification by

either multiple hydrogen bonds, nanoparticles or polymer; this strategy is called the "oligomer approach." However, the power conversion efficiencies of DSCs based on SPE are still much lower than those of the corresponding cells with liquid electrolyte due to diffusion limitations[8, 9] and poor interfacial contact with dyes.

Furthermore, a light-scattering layer with large nano-particles was effectively employed to enhance light harvesting and improve the efficiency of the solar cell.[10-12] Light-scattering effects can be maximized by controlling the particle size and the refractive index of the scattering layer materials, according to the Mie theory.[13]

In these contexts, we employ a submicron-sized (~ 500 nm) alumina bifunctional layer between two electrodes to solve the low ionic conductivity problem and also to improve the light harvesting efficiency.

The simplest way to solve the low ionic conductivity is to reduce the path length of ions, i.e., the thickness of the electrolyte, at a given ionic conductivity of I^-/I_3^- redox couples. However, when the path length is too short, shortage between two electrodes may occur. Therefore, we use a very thin insulating separator layer to prevent short-circuiting, consequently minimizing the thickness of the electrolyte layer, through which ions diffuse. In addition, the separator layer is made of a material that allows light-scattering effects in order to prolong the optical path length, which consequently improve the light harvesting efficiency. As a result, the power conversion efficiency of a DSC employing *solid state polymer electrolyte* was increased to 8.9 %, the highest ever reported, at 1 sun conditions.

[Experimental Details]

Preparation of working electrode

Fluorine-doped tin oxide (FTO) glass plates (Pilkington-TEC8) were cleaned using an ultrasonic bath of 2 vol. % Helmanex in D.I. water and ethanol. A doctor-bladed layer of 20-nm TiO_2 particles (PST-18 NR, CCIC) was used as photo-electrode. A 12-μm-thick transparent film and additional 4-μm scattering TiO_2 film (PST-400C, CCIC, particle size ~400 nm) were coated on the top of the conducting glass electrode. The TiO_2 electrodes were heated at 450 °C for 30 min. The TiO_2-coated

electrodes were treated with a 0.5 mM $TiCl_4$ solution for 20 min at 70 °C, followed by an annealing process for 30 min at 450 °C. Next, an alumina paste containing 500-nm Al_2O_3 particles was doctor-bladed to prepare a scattering layer on the TiO_2 film electrode. Following the heat treatment, these electrodes were immersed into the 0.3 M Z991 dye solution in acetonitrile (AN, 99.8+%, WAKO)/tert-butylalcohol (tBuOH, >99.5%, Sigma-Aldrich) (1/1, volume ratio) with 0.3 M bis-(3, 3-dimethyl-butyl)-phosphinic acid (DINHOP, Dyesol) and were kept at room temperature. The C106-D131 co-sensitized electrode was prepared as reported elsewhere.[14] The TiO_2 electrodes were rinsed with AN and dried. The Pt electrode was prepared by spin-coating 10 mM H_2PtCl_6 (99.995%, Sigma-Aldrich) in 2-propanol (anhydrous, 99.5%, Sigma-Aldrich) and was then sintered at 450 °C for 30 min. The dye-sensitized TiO_2 active area was 0.25 cm^2.

Al_2O_3 paste preparation

To prepare the alumina paste, 10 g of Al_2O_3 (500 nm, CNvision) was mixed with 35 g of α-terpineol (95%, TCI), 0.1 g of lauric acid (>98%, Sigma-Aldrich) and 5 g of ethyl-cellulose (46 cP, Sigma-Aldrich). After mixing each component, the paste was sonicated with stirring for 24 hours.

Electrolyte preparation

Solid polymer electrolyte (SPE) was composed of 2.0 M 1-methyl-3-propylimidazolium iodide (MPII, >98%, Sigma-Aldrich), 0.8 M iodine (>98%, Sigma-Aldrich), 0.1 M potassium iodide (KI, 99%, Sigma-Aldrich) and 0.5 M tert-buthylpyridine (tBP, 95%, Sigma-Aldrich) dissolved in a 6/4 (w/w) mix of poly(ethylene glycol)dimethylether (PEGDME, M.W. 500, Sigma-Aldrich)/poly(ethylene oxide) (PEO, M.W. 600,000, Sigma-Aldrich). The liquid electrolyte was composed of 0.6 M MPII, 0.05 M I_2, 0.5 M tBP and 0.1 M KI in AN. The additive electrolyte included 0.1 M lithium perchlorate ($LiClO_4$, 99.99%, Sigma-Aldrich) and 0.1 M guanidine thiocyanate (GuSCN, >99%, Sigma-Aldrich) on SPE.

Fabrication of DSCs

To fabricate **P10** and **P45** solar cells, Surlyn (25 and 60 μm, Dupont) was attached to the dye-coated TiO_2 electrode, and a counter electrode was pressed at 90 ℃ for 5 seconds with SPE into a sandwich-

type cell. Cell **P0** was prepared by pressing the cell consisting of SPE without Surlyn sandwiched between the dye-coated TiO_2 electrode and the counter electrolyte at 90 ℃ for 5 seconds. Cell **L** was fabricated with the dye-coated TiO_2 electrode and the counter electrode using 25-μm Surlyn, and the electrolyte was added through the holes on the counter electrode.

Characterization

The current-voltage (J-V) characteristics of DSCs were measured with a Keithley Model 2400 source meter and a solar simulator, with a 300 W Xenon arc-lamp (Newport) under 1 sun illumination (AM 1.5, 100 mW/cm^2). A light shading mask, placed on the residual area of the front side of the FTO substrate (except for the 0.25 cm^2 TiO_2 active area), was employed to prevent overestimation of the power conversion efficiency. The interfacial properties were characterized by electrochemical impedance spectroscopy (EIS) using an IM6 (Zahner) in the dark. A bias potential of 0 V was applied between the two electrodes, and the frequency range varied from 1 M to 10 mHz at a fixed amplitude of 10 mV. The photocurrent transient was measured by on-off irradiation under 1 sun illumination. The quantum efficiency of DSCs was measured as incident photon-to-current conversion efficiency (IPCE) (PV Measurements, Inc.). The transmittance spectra of the resulting scattering films were collected on a Jasco V-670 UV-Vis-NIR.

[Results and Discussion]

Figure 1 shows the *J-V* characteristics of DSCs using the liquid and SPEs based on the Z991 dye with varying cell gap, measured under 1 sun conditions (AM 1.5 G and 100 mW cm^{-2}) (Table S1). Cell **L** (liquid electrolyte-based device with a 25-μm spacer) shows higher photovoltaic efficiency than **P0**, **P10** and **P45** (SPE-based devices with 0-, 25- and 60-μm spacer, respectively). Among the SPE-based devices (**P** series), the photocurrent density and the energy conversion efficiency monotonically increase with a decrease in the thickness of the electrolyte layer (**P0** < **P10** < **P45)**, whereas the open circuit voltage decreases marginally. When the thickness of the bulk electrolyte layer, **T**, as defined in Scheme 1, becomes zero (**P0**), the ion diffusion distance is shortened, resulting

in an increase in J_{SC}, giving rise to an overall efficiency of 8.2 % with SPE, which appears to be the highest ever reported among DSCs employing polymer electrolyte.

A previous study showed that the low current density through PEO-based SPEs was mostly attributable to its low ionic conductivity, from 10^{-4} to 10^{-6} S/cm.[15] In PEO-based SPEs unlike liquid electrolyte, ions are dissociated by the polymer matrix and can be transported through the free volume of the matrix, assisted by polymer segmental motion.[16] In other words, the current density appears to be diffusion-limited.[17] Surprisingly, **P0** with ionically low conductive polymer electrolyte shows similar photocurrent decay behavior to that of liquid **L,** as shown in Figure 2, whereas both **P10** and **P45** show significant photocurrent decay. This may be attributable to the increased ion flux through the solid electrolyte layer, which was achievable by reducing the polymer electrolyte layer thickness according to Fick's law, equation (1):

$$J = D\,\Delta C/L \qquad (1)$$

where J is ionic flux, D is diffusion coefficient, ΔC is ion concentration difference and L is electrolyte layer thickness. In other words, the ion flux, J, will be increased with the decrease in the electrolyte layer thickness, L, for a given architecture with a constant diffusion coefficient D and a given concentration difference, ΔC.[18] These results demonstrate that the ion diffusion limitation for **P0** is nearly overcome by reducing the thickness of the bulk polymer electrolyte layer, **T**.

Figure 3 shows Nyquist plots of the symmetric cell made using Pt electrodes. The semicircle in the high-frequency region corresponds to the charge-transfer process of the electrolyte/electrode interface.[19] The series resistance (R_S) and charge-transfer resistance (R_{ct}) in **P0** are 6.0 Ω and 2.4 Ω, respectively, which are smaller than those of **P10** and **P45**, indicating the strong thickness-dependent resistance behavior. The semicircle in the low-frequency region is assigned to the Nernst diffusion process of triiodide ions.[20-22] **P0** shows a small Warburg diffusion resistance (Z_W) (2.2 Ω) owing to low limited ion diffusion.[23-25] Consequently, the overall impedance of the **P0** is very close to that of **L**, resulting in comparable photovoltaic performance.

The light-scattering effects of the alumina layer can be evaluated by measuring the transmittance properties of the films. Figure 4 shows the UV-vis transmittance spectra of different films with

various scattering layers based on a 12-μm transparent TiO_2 film in the range of visible light. There were four different working electrodes prepared for this research. A reference 12-μm-thick electrode, prepared from the standard CCIC 18-nm TiO_2 paste, was labeled **R.** Electrode **RT** had a 4-μm scattering layer consisting of 400-nm mesoporous TiO_2 particles on top of the **R** film. A 500-nm-sized 4-μm alumina layer was coated on top of the **R** film to make a **RA** working electrode. The last film was **RTA**, which was made from another 4-μm alumina layer on a **RT** film. Cell **R** has the highest light transmittance due to the absence of a light scattering layer. The scattering effect of the TiO_2 layer with 400-nm particles (**RT**) is higher than that of the Al_2O_3 layer with 500-nm nanoparticles (**RA**). This could be caused by the smaller reflective index of alumina than that of TiO_2[26] because the scattering effect is related to particle size and the difference in reflective index between particle and medium.[27] All electrodes have nearly zero transmittance in the short wavelength range (from 400 to 550 nm). When both scattering layers of TiO_2 and Al_2O_3 were introduced (**RTA**), the transmittance of light in the wavelengths longer than 600 nm was significantly suppressed. As shown in Figures S2 and S3, both **RT** and **RTA** cells showed a significant increase in IPCE over the long-wavelength range (600-750 nm) compared to the reference cell **R**. This enhancement is attributed to the scattering effect of the 400-nm TiO_2 particles in **RT** and **RTA.** Although the cell with an alumina layer also had a strong back-scattering effect, the **RT** cell had a higher IPCE than the **RA** cell in the long-wavelength range. In the cases of the liquid electrolyte based DSCs as shown in Figure S4 and S5, the short-circuit current and IPCE are also slightly increased with addition of alumina scattering layer. These results demonstrate that the Al_2O_3 layer helps increase the light harvesting efficiency and the energy conversion efficiency.

To verify the potential of **P0**, we further optimized the solid-state DSC by additional introduction of additives in SPE, such as GuSCN and $LiClO_4$,[28] and by co-sensitization of C106 and D131.[14] When C106 and D131 were co-sensitized with GuSCN and $LiClO_4$, the J_{SC} value greatly improved to 21.0 mA cm^{-2}, and the power conversion efficiency reached 8.9 % (one sun illumination) with V_{OC} and *FF* values of 0.68 V and 0.62, respectively. The *J-V* characteristics of the optimized solid-state DSC under AM 1.5 G are shown in Figure 5, and the resulting cell parameters are listed in the inset. This

efficiency is significantly higher than those reported for other solid-state DSCs using solid-state polymer electrolytes (e.g., P. Falaras et al., 6.55 %).[29]

[Figures and Tables]

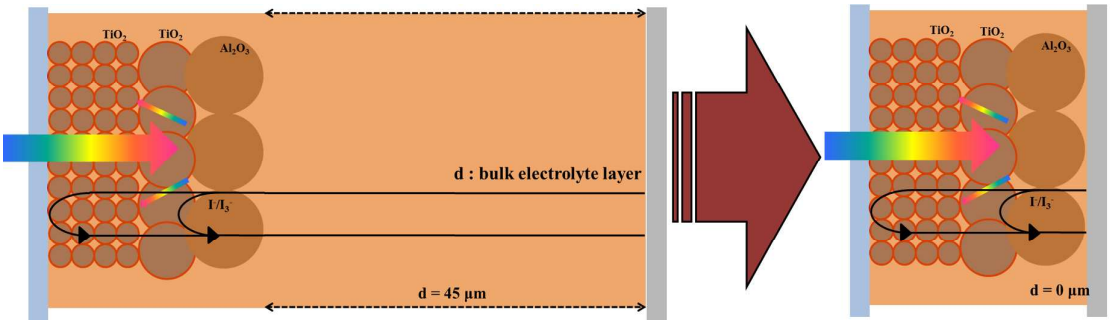

Scheme 1. Scheme representing DSCs for reduction of the bulk electrolyte layer thickness, d, (a) d= 45 μm (**P45**) and (b) d=0 μm (**P0**) with a bifunctional insulating Al_2O_3 layer (~ 4 μm thick).

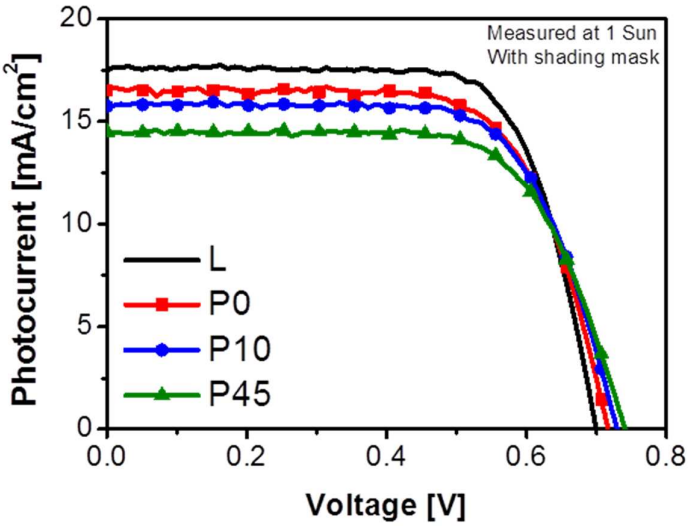

Figure 1. *J-V* characteristics of DSCs based on liquid (**L**) and solid-state polymer (**P** series) electrolytes using an alumina layer with varied thickness of the bulk electrolyte layer from 0 to 45 μm under 1 sun conditions (AM 1.5 irradiation with 100 mW/cm^2). Active area of the devices when the shading mask was 0.25 cm^2.

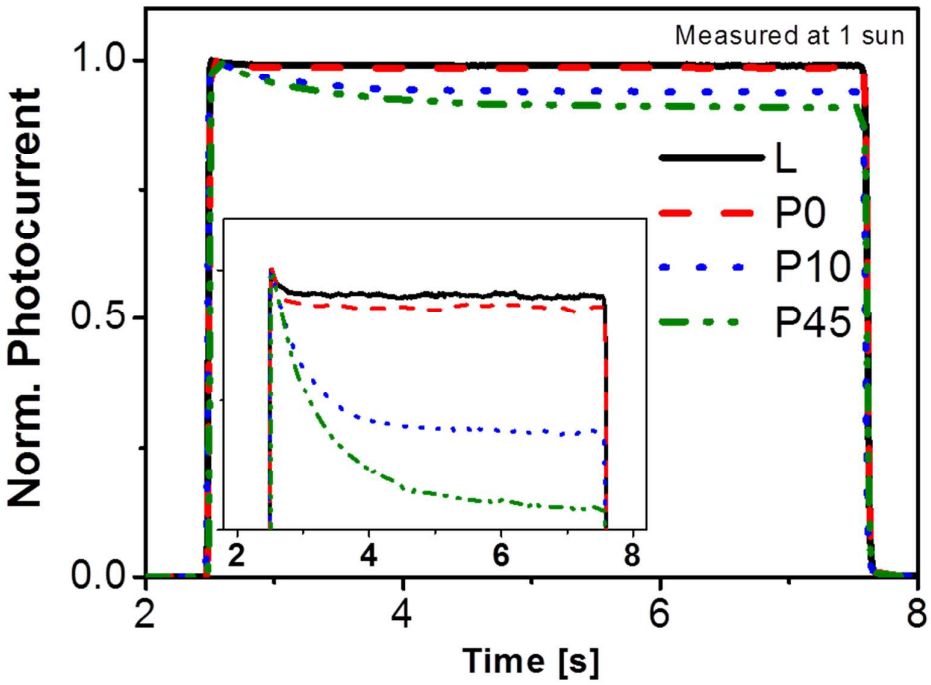

Figure 2. Photocurrent transients of DSCs with an alumina layer with varied thickness of the bulk electrolyte layer under 1 sun conditions. The photocurrent was normalized with the initial value. The inset in the figure is the expanded part of photocurrent decay over a short period.

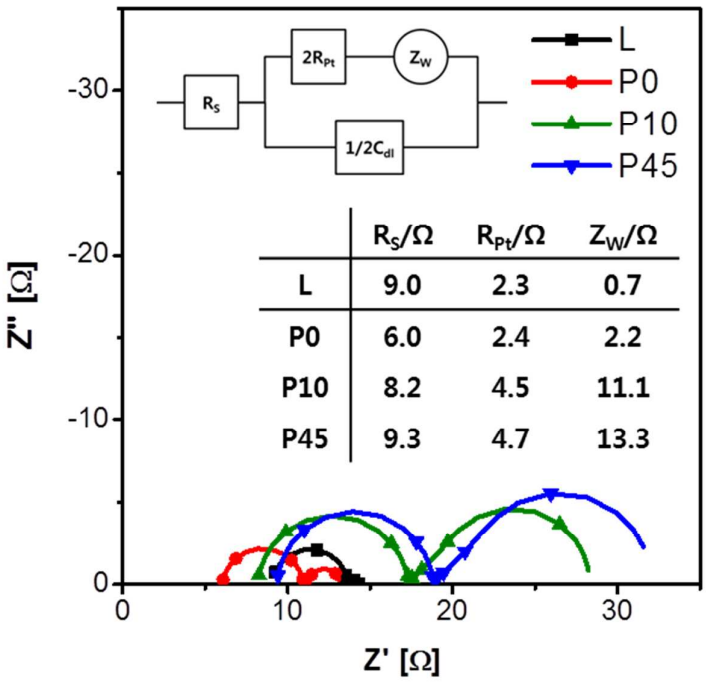

	R_S/Ω	R_{Pt}/Ω	Z_W/Ω
L	9.0	2.3	0.7
P0	6.0	2.4	2.2
P10	8.2	4.5	11.1
P45	9.3	4.7	13.3

Figure 3. Nyquist plots measured under a 0 V bias for symmetric cells with varied distance between Pt-coated electrodes. The inset figure and table show equivalent circuit and series resistance (R_s), charge transfer resistance (R_{Pt}), constant of phase element (C_{dl}) and Warburg diffusion resistance (Z_W) of the symmetric cells.

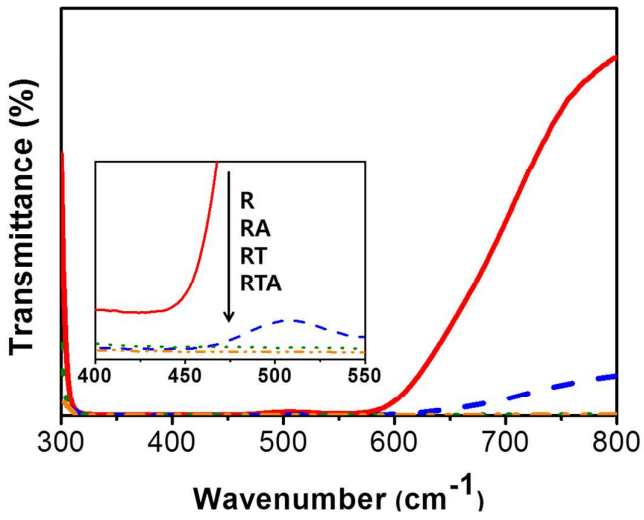

Figure 4. UV-vis spectra of transmittance from different electrodes corresponding to reference (**R**), as

a transparent reference TiO_2 without a scattering layer, and with alumina (**A**) and titania (**T**) layers. The inset in the figure is the expansion of transmittance from 400 to 500 nm.

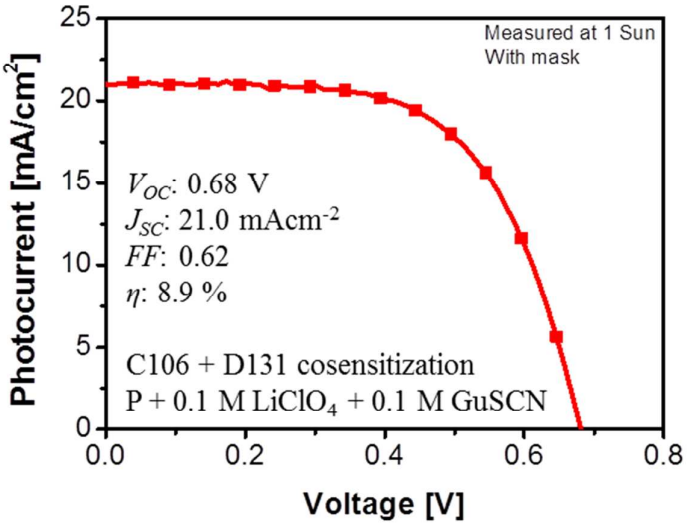

Figure 5. *J-V* characteristics of DSCs based on solid-state polymer electrolyte using co-sensitization and electrolyte additives under 1 sun conditions (AM 1.5 irradiation with 100 mW/cm^2). Active area of the devices with a shading mask was 0.25 cm^2. The inset in the figure shows the photovoltaic parameters of the DSCs.

[Conclusion]

We introduced a bifunctional alumina layer having both separator and scattering functions for solid-state DSC employing polymer electrolyte, resulting in a very high overall energy conversion efficiency of 8.2 % under 1 sun conditions. This can be achieved by minimizing the thickness of the electrolyte layer and therefore reducing the travel length of I^-/I_3^- with a low-diffusion polymer electrolyte. Through the photocurrent transient and EIS data, the limitation of ionic conductivity was reduced by decreasing the thickness of the SPE. DSCs based on an alumina layer without a spacer showed the highest energy conversion efficiency due to the light-scattering effects and the reduced limitation of ion diffusion by shortening the ion diffusion distance. Shortening the ion diffusion length is likely to become important in the quest for high-performance SPE-based DSCs in order to achieve high performance and long-term stability in commercial applications.

[References]

1. A. Yella, H.-W. Lee, H. N. Tsao, C. Yi, A. K. Chandiran, M. K. Nazeeruddin, E. W.-G. Diau, C.-Y. Yeh, S. M. Zakeeruddin and M. Grätzel, *Science*, 2011, **334**, 629-634.
2. Z. Yu, N. Vlachopoulos, M. Gorlov and L. Kloo, *Dalton Transactions*, 2011, **40**, 10289-10303.
3. N. Papageorgiou, Y. Athanassov, M. Armand, P. Bonho, H. Pettersson, A. Azam and M. Grätzel, *J. Electrochem. Soc.*, 1996, **143**, 3099-3108.
4. Y. Saito, N. Fukuri, R. Senadeera, T. Kitamura, Y. Wada and S. Yanagida, *Electrochem. Commun.*, 2004, **6**, 71-74.
5. I. Ding, N. Tétreault, J. Brillet, B. E. Hardin, E. H. Smith, S. J. Rosenthal, F. Sauvage, M. Grätzel and M. D. McGehee, *Adv. Funct. Mater.*, 2009, **19**, 2431-2436.
6. M. Shaheer Akhtar, J.-M. Chun and O. Yang, *Electrochem. Commun.*, 2007, **9**, 2833-2837.
7. Y. Zhou, W. Xiang, S. Chen, S. Fang, X. Zhou, J. Zhang and Y. Lin, *Chem. Commun.*, 2009, 3895-3897.
8. C.-L. Chen, H. Teng and Y.-L. Lee, *J. Mater. Chem.*, 2011, **21**, 628-632.
9. J. E. Benedetti, A. D. Gonçalves, A. L. Formiga, M.-A. De Paoli, X. Li, J. R. Durrant and A. F. Nogueira, *J. Power Sources*, 2010, **195**, 1246-1255.
10. Z.-S. Wang, H. Kawauchi, T. Kashima and H. Arakawa, *Coord. Chem. Rev.*, 2004, **248**, 1381-1389.
11. S. Hore, P. Nitz, C. Vetter, C. Prahl, M. Niggemann and R. Kern, *Chem. Commun.*, 2005, **0**, 2011-2013.
12. J.-H. Yoon, S.-R. Jang, R. Vittal, J. Lee and K.-J. Kim, *Journal of Photochemistry and Photobiology A: Chemistry*, 2006, **180**, 184-188.
13. F. Huang, D. Chen, X. L. Zhang, R. A. Caruso and Y.-B. Cheng, *Adv. Funct. Mater.*, 2010, **20**, 1301-1305.
14. L. H. Nguyen, H. K. Mulmudi, D. Sabba, S. A. Kulkarni, S. K. Batabyal, K. Nonomura, M. Gratzel and S. G. Mhaisalkar, *Phys. Chem. Chem. Phys.*, 2012, **14**, 16182-16186.
15. M.-S. Kang, J. H. Kim, J. Won and Y. S. Kang, *The Journal of Physical Chemistry C*, 2007, **111**, 5222-5228.
16. A. F. Nogueira, C. Longo and M. A. De Paoli, *Coord. Chem. Rev.*, 2004, **248**, 1455-1468.
17. B. M. Klahr and T. W. Hamann, *The Journal of Physical Chemistry C*, 2009, **113**, 14040-14045.
18. W. F. Smith and J. Hashemi, *Foundations of materials science and engineering*, Mcgraw-Hill Publishing, 2006.
19. F. Fabregat-Santiago, J. Bisquert, E. Palomares, L. Otero, D. Kuang, S. M. Zakeeruddin and M. Grätzel, *The Journal of Physical Chemistry C*, 2007, **111**, 6550-6560.
20. E. Ramasamy, W. J. Lee, D. Y. Lee and J. S. Song, *Electrochem. Commun.*, 2008, **10**, 1087-1089.
21. A. Kay and M. Grätzel, *Sol. Energy Mater. Sol. Cells*, 1996, **44**, 99-117.

22. L. Han, N. Koide, Y. Chiba, A. Islam, R. Komiya, N. Fuke, A. Fukui and R. Yamanaka, *Appl. Phys. Lett.*, 2005, **86**, -.
23. M. S. Góes, E. Joanni, E. C. Muniz, R. Savu, T. R. Habeck, P. R. Bueno and F. Fabregat-Santiago, *The Journal of Physical Chemistry C*, 2012, **116**, 12415-12421.
24. I. Hod, Z. Tachan, M. Shalom and A. Zaban, *The Journal of Physical Chemistry Letters*, 2011, **2**, 1032-1037.
25. A. Zaban, J. Zhang, Y. Diamant, O. Melemed and J. Bisquert, *The Journal of Physical Chemistry B*, 2003, **107**, 6022-6025.
26. R. D. Shannon, R. C. Shannon, O. Medenbach and R. X. Fischer, *J. Phys. Chem. Ref. Data*, 2002, **31**, 931-970.
27. C. Lu and B. Yang, *J. Mater. Chem.*, 2009, **19**, 2884-2901.
28. J. Zhang, Y. Cui, X. Zhang, Q. Sun, J. Zheng, P. Wang, J. Feng and Y. Zhu, *Comptes Rendus Chimie*, 2013, **16**, 195-200.
29. P. Falaras, T. Stergiopoulos and D. S. Tsoukleris, *Small*, 2008, **4**, 770-776.